19th Australasian Fluid Mechanics Conference
Melbourne, Australia
8-11 December 2014

Linear Stability Analysis of Horizontal Convection Forced Radially in a Rotating Cylindrical Enclosure

Wisam K. Hussam, Tze K. Tsai and Gregory J. Sheard

The Sheard Lab, Department of Mechanical and Aerospace Engineering
Monash University, Melbourne, Victoria 3800, Australia

Abstract

The effect of rotation on the three-dimensional instability of a horizontal convection flow in a free-surface cylindrical enclosure driven by a radially increasing temperature over the base is numerically investigated using a linear stability analysis. The results demonstrate that higher rotation rates serve to inhibit the onset of non-axisymmetric instability. Two distinct instability modes are found. A low-wavenumber mode with azimuthal wavenumber 5 is found exhibiting spiral structures extending out from the axis and deep into the enclosure consistent with baroclinic instability, a high-wavenumber mode is also observed, which is localised near the buoyant end of the base. That disturbance exhibits features consistent with a Rayleigh-Bénard type azimuthal roll instability in the radial horizontal convection boundary layer.

Introduction

The flows driven by a temperature difference imposed along a horizontal boundary is known as horizontal convection [3]. This is in contrast to Rayleigh–Bénard convection in which the temperature difference is in the vertical direction [6]. Uneven heating applied across a horizontal boundary occurs in myriad geophysical and industrial systems, motivating further study into horizontal convection. In addition, the effect of rotation on convection flows is important in many industrial applications as well as in astrophysical and geophysical flows, including circulations of atmospheres, and the interiors of planets and stars [8]. In fact, for rapidly rotating, stratified fluids that are subjected to horizontal temperature gradients, baroclinic instability may originate as unstable wave-like disturbances [7]. The combination of a radially forced horizontal convection and rotation in a cylindrical enclosure idealizes features of geophysical flows such as polar vortices in which solar heating of the surface has a latitudinal dependence, and this forms the basis of the system considered in the present study.

For non-rotating horizontal convection at high Rayleigh number, [11] demonstrated that the horizontal thermal layer has a thickness proportional to $Ra^{-1/5}$. However, in a rapidly rotating system, the thinnest horizontal boundary layer is Ekman layer. Therefore, the ratio of thw thickness of these layers will be important in describing the flow.

The effects of rotation on horizontal convection have been investigated by [2, 1, 4]. The dynamics of a horizontal convection in a rotating annuls have been investigated experimentally by Hignett etal [2]. The enclosure was rotated around its central axis in which a radial temperature gradient is maintained along the lower boundary in all directions from the axis. The dynamics of the flow is described in terms of a non-dimensional parameter Q, which is defined as the square of the ratio of non-rotating thermal layer scale to Ekman layer scale. Their experiments focused on the rotating regime with $Q \sim O(1)$. For a large Rayleigh number, six flow regimes were determined depending on the magnitude of parameter Q. They found that for small Q, the flow is only weakly modified by rotation, and the scaling law for heat flux and thermal boundary layer is similar to the non-rotating case (i.e. Rossby scaling for horizontal convection). Also, a critical value of $Q_c \approx 3.4$ was determined beyond which baroclinic instability and waves were predicted.

Experiments on thermal convection in annular geometry showed that when the rotation rate exceeds a certain critical value Q_c, Coriolis forces inhibit overturning motion in meridian plane and promote a sloping convection or baroclinic waves flow. In such flow, although the temperature difference is imposed primarily along a horizontal boundary, at equilibrium the resulting temperature surfaces will be inclined. This implies that for potential energy to release, which has the possibility to amplify a perturbation by converting potential energy to kinetic energy, there must be a slope between the isothermal surfaces and the horizontal [7]. The linear stability analysis on analytical solution performed by Barkan etal [1] showed that the sloping isopycnals of rapidly rotating horizontal convection flow results in greatly enhanced available potential energy and hence the flow is expected to be baroclinically unstable.

A key question relating to rotating horizontal convection (RHC) flow is its stability to axisymmetric and non-axisymmetric disturbances. To address this question, this study performs a global linear stability analysis by obtaining the eigenvalue solution arising from the linearization of the governing incompressible Navier–Stokes equations coupled to a buoyancy transport equation through the Boussinesq approximation.

Numerical Model and Methodology

The system under consideration consists of a free surface cylindrical enclosure rotating with an angular velocity Ω. It is filled with fluid, and a radially increasing linear temperature profile is imposed on the base. The tank radius R and height H combine to define an aspect ratio which in this study is fixed at $H/R = 0.4$. The system is depicted in figure 1.

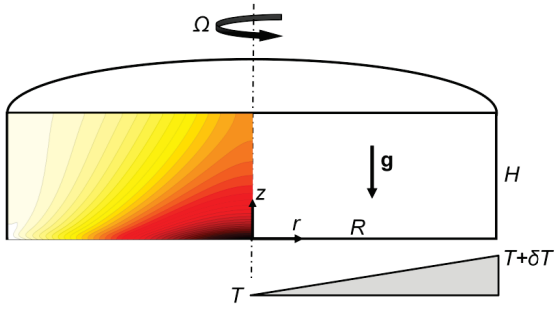

Figure 1. Schematic representation of the system, showing key symbols. Representative contours of temperature are plotted on the computational domain spanning the meridional semi-plane.

The azimuthal velocity imposed on the impermeable base and

side wall is $u_\theta = r\Omega$, where r is the radial coordinate. To model a free surface, a stress-free condition is imposed on the top boundary ($u_z = \partial u_r/\partial z = \partial u_\theta/\partial z = 0$). The side wall is thermally insulated by imposition of a zero normal temperature gradient, and to simplify the computational model, no heat loss is permitted through the stress-free top surface, which is also approximated as being thermally insulated. The linear temperature profile increases by δT from $r = 0$ to $r = R$ along the base to drive horizontal convection in the z–r plane.

A Boussinesq approximation for fluid buoyancy is employed, in which density differences in the fluid are neglected except through the gravity term in the momentum equation. Under this approximation the energy equation reduces to a scalar advection-diffusion equation for temperature which is evolved in conjunction with the velocity field. The fluid temperature is related linearly to the density via a thermal expansion coefficient α.

The dimensionless Navier–Stokes and energy equations governing a Boussinesq fluid may be written as

$$\nabla \cdot \mathbf{u} = 0, \tag{1}$$

$$\frac{\partial \mathbf{u}}{\partial t} = \mathbf{N_1} - \nabla p + \frac{QRa^{2/5}}{2}\nabla^2 \mathbf{u} + \mathbf{g}T\frac{4Ra^{1/5}}{PrQ^2}, \tag{2}$$

$$\frac{\partial T}{\partial t} = \mathbf{N_2} + \frac{2}{PrQRa^{2/5}}\nabla^2 T, \tag{3}$$

where $\mathbf{N_1} = -(\mathbf{u}\cdot\nabla)\mathbf{u}$, $N_2 = -(\mathbf{u}\cdot\nabla)T$. $\mathbf{u}$, p, t, Q, Pr, $\mathbf{g}$ and T are the velocity vector, kinematic static pressure, time, rotation rate, Prandtl number, a unit vector in the direction of gravity, and temperature, respectively. In equations (1)-(3), lengths have been scaled by R, velocities by $R\Omega$, time by Ω^{-1}, and temperature by δT (the imposed temperature difference across the bottom wall).

A horizontal Rayleigh number characterizing the thermal forcing is given by

$$Ra = \frac{g\alpha\delta T R^3}{\nu\kappa_T}, \tag{4}$$

where g is the gravitational acceleration and κ_T is the thermal diffusivity of the fluid.

The rotation rate is characterised as the square of the thermal boundary layer thickness and Ekman layer thickness [2],

$$Q = \frac{1}{ERa^{2/5}}, \tag{5}$$

where E is the Ekman number characterizing the ratio of viscous to Coriolis forces [2],$E = \nu/2\Omega R^2$. This ratio accounts for the importance of rotation in horizontal convection. When $Q > O(1)$, a thermal boundary layer is thicker, and rotation is important. When $Q < O(1)$, the Ekman boundary layer is thicker than a thermal boundary layer, and frictional dissipation is important within the thermal boundary layer.

The Prandtl number of the fluid is given as

$$Pr = \frac{\nu}{\kappa_T}, \tag{6}$$

and throughout this study $Pr = 6.14$, which approximates water at laboratory conditions.

The governing flow and energy equations (2)-(3) are solved in cylindrical coordinates using a nodal spectral-element method in space, and a third-order scheme based on backwards differentiation is employed for time integration [5]. The cylindrical formulation of the solver employed here has been validated and used recently to study a rotating horizontal convection system by Hussam etal [4]. A grid independence study determined that integrated Nusselt numbers [4] were independent of resolution with a polynomial order of 7, which is used hereafter.

To consider different types of instability, a Rayleigh number ($O(10^9)$) and rotation rates ($1 \leq Q \leq 30$) are considered in this study.

Linear Stability Analysis Technique

The potential for non-axisymmetric three-dimensional instability developing and significantly altering its characteristics on an axisymmetric base flow motivies an application of linear stability analysis. In this analysis, the velocity, pressure and temperature are decomposed into the sum of an axisymmetric field ($\bar{\mathbf{u}}$, $\bar{\mathbf{P}}$, $\bar{T}$) and a small non-axisymmetric perturbation field ($\mathbf{u}'$, $\mathbf{P}'$, T'). The perturbation field is constructed as a single complex Fourier mode of an azimuthal expansion of the flow field and the wavenumber of the perturbation is a parameter in the stability analysis. Substituting these onto equations (1)-(3) and eliminating terms satisfying equations (1)-(3) for axisymmetric flow as well as products of perturbation quantities yield the linearized Navier–Stokes and energy equations. A linear stability analysis is performed to calculate the Floquet multipliers of the system. The Floquet multipliers correspond to the dominant eigenvalues of an evolution operator associated with time integration of the linearized equations, and are related to the exponential growth rate of individual wavenumbers through $\mu = \mathbf{e}^{\sigma T}$, where σ represents the growth rate and T is the time interval over which the equations are integrated within the eigenmode solver. The growth rate is evaluated from $\sigma = \log(\mu)/T$. In the case of steady-state base flows, such as are produced in the present study, T may be arbitrarily chosen. The stability of the base flow is then determined from dominant eigenvalues with the largest modulus. If $|\mu| > 1$, then the flow is unstable, and if $|\mu| < 1$, the flow is stable. Neutral stability occurs when $|\mu| = 1$, which represents a system in which the perturbation will neither grow nor decay.

Results and Discussion

Flow Structure in the Weak and Strong Rotation Regimes

In order to illustrate the effects of rotation, figure 2(a,b,c) plots the axisymmetric temperature field at different rotation rates. If the rotation rate is not too high, i.e. $Q \sim O(1)$, then a little change from the non-rotating case is expected. For $Q = 1$, figure 2(a), the temperature field is similar to the non-rotating field, in agreement with experimental results of Hignett etal [2] and numerical results of Barkan etal [1] and Hussam etal [4]. However, for $Q = 25$, there is a significant difference with no apparent thermal boundary layer. Away from the side wall, there is an extensive region in which the temperature isolines touch both top and bottom boundaries as shown in figure 2(c). For $Q = 5$ (figure 2(b)), more of the thermal isolines no longer intersect with the bottom boundary, inconstant to the that of $Q = 25$. Also, it can be noted that for $Q \sim O(1)$ the forcing boundary follows Rossby scaling [11] (dashed line) while it follows Stern scaling [12] (dash-dot-dot) for high rotation rates.

Global Instability Modes

The growth rates over a wide range of wavenumbers for $Ra = 10^9$ and different rotations rate is depicted in figure 3. For $5 \leq Q \leq 15$, two mode peaks comprising low and high wavenumbers which are referred to as Modes I and II, respectively, can be seen in the $\sigma - k$ plane. Local maxima typically rep-

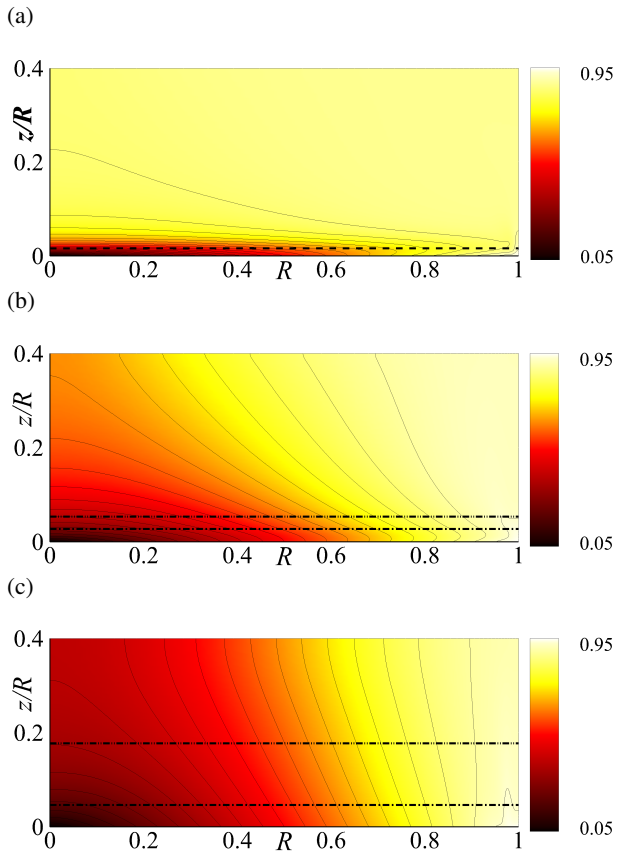

Figure 2. Contour plots of temperature at (a) $Q = 1$, (b) $Q = 5$, and (c) $Q = 25$ for Rayleigh numbers $Ra = 10^9$, plotted on a meridional cross-section through the centre of the tank. Dashed, dot-dashed and dash-dot-dot lines represent thermal boundary layer depth provided by Rossby [11], Park & Whitehead [9] and Stern [12], respectively.

resent distinct instability modes. Asymptotically the growth rate decreases monotonically for wavenumbers beyond these peaks. However, for $Q = 25$, only a single peak comprising low wavenumbers is found. Also, for this $Q-$ range, the profiles do not change significantly with varying Q, though the range of wavenumbers over which the maximum growth are detected changes. For example, the mode branches cover $2 \leq k \leq 25$ for $Q = 5$, while a larger range of $5 \leq k \leq 50$ is seen for $Q = 10$.

To elucidate the variation of maximum growth rate with rotation rate, figure 4 displays data extracted from figure 3. It can be seen that both the low and high wavenumber instability growth rates first increase then decrease with increasing Q. A maximum peak can be seen at $Q \approx 5$ and 10 with the most unstable wavenumber predicted as $k_{\text{peak}} \approx 5$ and 25 for the low and high wavenumbers, respectively.

In figure 5 we plot the marginal stability curve for rotation rates up to 30. Everywhere inside the curve the growth rate is positive and hence the flow is linearly unstable. Points along the curve were obtained by locating the zero crossings of growth rate branches as a function of k for rotation rate between 1 and 30. The flow is unstable for rotation rates $Q \gtrsim 1$. It can be noted that with increasing rotation rate, the envelope of unstable wavenumbers initially increases very rapidly as both the baroclinic and horizontal convection modes develop. Beyond $Q \approx 15$ the envelope shrinks to lower wavenumbers. Evidently the horizontal convection mode is suppressed at high rotation rates.

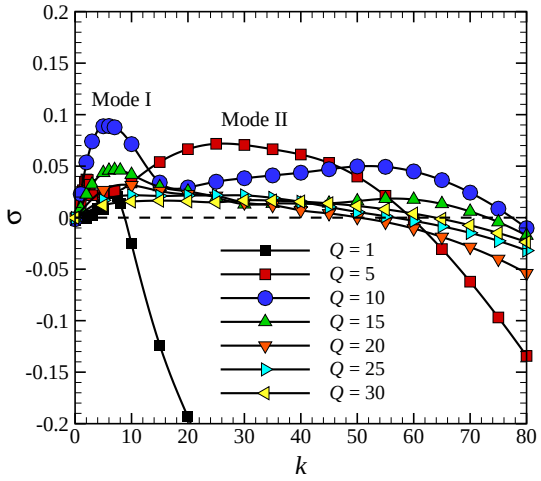

Figure 3. Growth rate σ as a function of azimuthal wavenumber k for varies rotation rate Q. Two mode peaks of σ are present at low and high wavenumbers, respectively. The dashed line represents the zero line where points above and below symbolize stable and unstable modes, respectively.

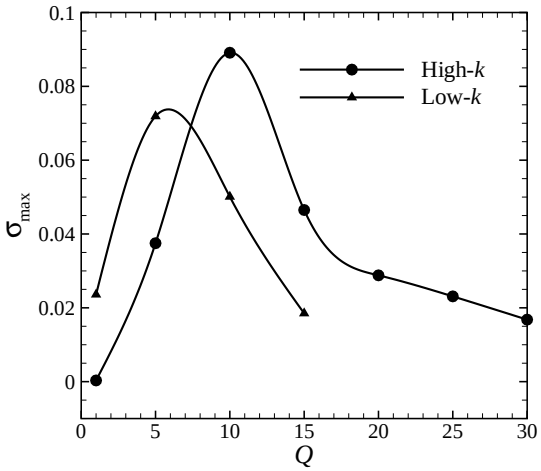

Figure 4. Maximum growth rate σ_{max} as a function of rotation rate Q for mode I and mode II as per figure 3.

An illustration of three-dimensional instability structures of modes I and II are shown in figure 6(a,b), respectively for $Q = 10$. It can be noted that mode I exhibits disturbances spanning vertically between the horizontal boundaries and located away from the lateral sides while mode II displays localized disturbances near the hot end of the base. Further elucidation of the azimuthal mode structures is shown in figure 6 by superimposing this perturbation field onto the axisymmrtric base flow. figure 6(a) demonstrates that mode I exhibits spiral structures extending out from the axis and deep into the enclosure (consistent with baroclinic instability [7]). For mode II figure 6(b), the disturbance exhibits features consistent with Rayleigh-Bénard type azimuthal instability in the radial horizontal convection boundary layer where mode manifests as azimuthal rolls within the forcing boundary layer.

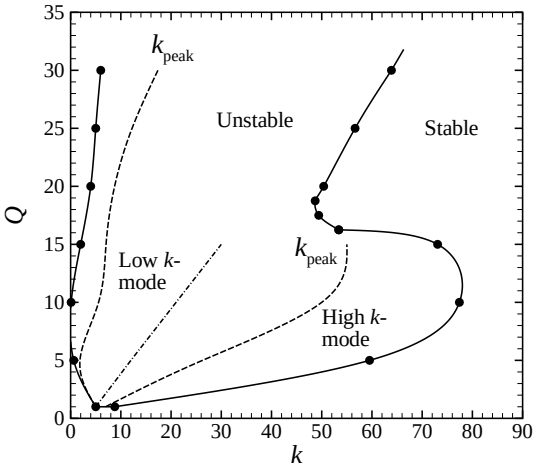

Figure 5. Marginal stability plot of rotational rate Q against azimuthal wavenumbers k for $Ra = 10^9$. Dashed and dash-dot lines show the locus of maximum growth rate as a function of k and the threshold between eigenvalues associated with low-k and high-k, respectively.

(a) $k = 5$

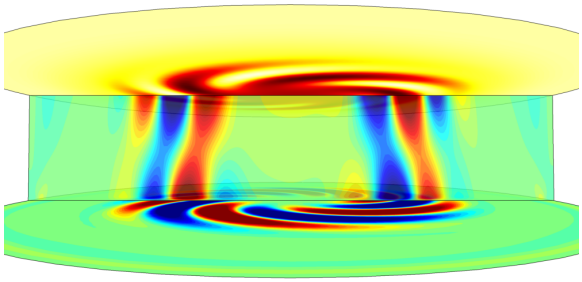

(b) $k = 25$

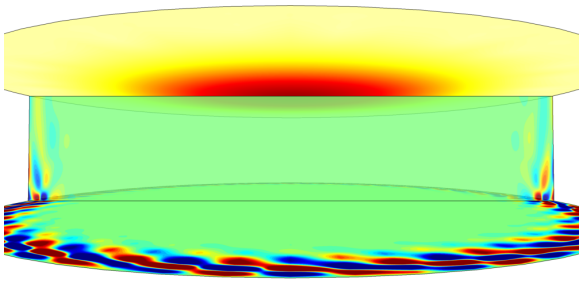

Figure 6. Contours of z vorticity of three-dimensional perturbation field for most unstable azimuthal wavenumbers as indicated (vertical plane), depicted on $r-z$ plane for $Q = 10$ and $Ra = 10^9$. Temperature contours are plotted on the top surface and θ-vorticity field on the base. The non-axisymmetric flow is constructed by superposition of the base flow and linear stability mode as per figure 3.

Conclusion

We have investigated the effect of rotation parameter at high Rayleigh number on the three-dimensional instability in horizontal convection in a cylindrical enclosure, with horizontal convection forcing imposed radially. A spectral-element method was used both to obtain the axisymmetric base flow solutions and to evolve the linearized perturbation fields over a range of $1 \leq Q \leq 30$ and Rayleigh number 10^9. Two distinct instability modes are found. A short-wavenumber mode (mode I), with azimuthal wavenumbers 5, is found exhibiting spiral structures extending out from the axis and deep into the enclosure. A high-wavenumber mode (mode II) is also observed, which is localised near the buoyant end of the base. That disturbance exhibits features consistent with a Rayleigh-Bénard type azimuthal roll instability in the radial horizontal convection boundary layer.

Acknowledgements

This work is supported by ARC Discovery Grant DP120100153, and a high-performance computing time allocation through the National Computational Infrastructure (NCI) Merit Allocation Scheme and Monash SunGrid system through Monash e-Research Centre.

References

[1] Barkan, R., Winters, K. B. and Llewellyn Smith, S. G., Rotating horizontal convection, *Journal of Fluid Mechanics*, **723**, 2013, 556–586.

[2] Hignett, P., Ibbetson, A. and Killworth, P. D., On rotating thermal convection driven by non-uniform heating from below, *Journal of Fluid Mechanics*, **109**, 1981, 161–187.

[3] Hughes, G. O. and Griffiths, R. W., Horizontal convection, *Annu. Rev. Fluid Mech.*, **40**, 2008, 185–208.

[4] Hussam, W. K., Tsai, T. K. and Sheard, G. J., The effect of rotation on radial horizontal convection and Nusselt number scaling in a cylindrical container, *Int. J. Heat Mass Trans.*, **77**, 2014, 46–59.

[5] Karniadakis, G. E., Israeli, M. and Orszag, S. A., High-order splitting methods for the incompressible Navier–Stokes equations, *J. Comput. Phys.*, **97**, 1991, 414–443.

[6] King, E. M., Stellmach, S. and Aurnou, J. M., Heat transfer by rapidly rotating Rayleigh-Bénard convection, *J. Fluid Mech.*, **691**, 2012, 568–582.

[7] Lappa, M., *Rotating thermal flows in natural and industrial processes*, John Wiley & Sons, 2012.

[8] Marshall, J. and Schott, F., Open-ocean convection: Observations, theory, and models, *Rev. Geophys.*, **691**, 1999, 1–64.

[9] Park, Y.-G. and Whitehead, J., Rotating convection driven by differential bottom heating, *Journal of Physical Oceanography*, **29**, 1999, 1208–1220.

[10] Robinson, A. and Stommel, H., The oceanic thermocline and the associated thermohaline circulation1, *Tellus*, **11**, 1959, 295–308.

[11] Rossby, H. T., On thermal convection driven by non-uniform heating from below: an experimental study, in *Deep Sea Research and Oceanographic Abstracts*, Elsevier, 1965, volume 12, 9–16, 9–16.

[12] Stern, M. E., *Ocean circulation physics*, volume 246, Academic Press New York, 1975.